***Final Draft***
**of the original manuscript:**

Rodrigues, P.; Braz Fernandes, F.M.; Paula, A.S.; Oliveira, J.P.; Ribero, S.B.; Texeira, E.N.; Schell, N.:

**Microstructural characterization of NiTi shape memory alloy produced by rotary hot forging**

In: Powder Diffraction (2017) International Centre for Diffraction Data

DOI: 10.1017/S0885715617000549

# Microstructural Characterization of NiTi Shape Memory Alloy Produced by Rotary Hot Forging

P. Rodrigues[1a], F. M. Braz Fernandes[1], A.S. Paula[2,3], J.P. Oliveira[1], S.B. Ribeiro[4], E.N. Texeira[4], N. Schell

*[1]CENIMAT, Faculdade de Ciências e Tecnologia, Universidade Nova de Lisboa, Portugal;00*

*2Mechanical Engineering and Materials Department-SE-4, Instituto Militar de Engenharia–IME, Brazil;*

3*Metallurgical Engineering Post-Graduation Program (PPGEM), Universidade Federal Fluminense (UFF), Brazil.;*

*4Centro Universitário de Volta Redonda - UNIFOA, Brazil;*

*5HZG, Geesthacht, Germany.*

The thermomechanical processing of NiTi shape memory alloys usually involves several steps of hot and/or cold deformation. The present work presents the structural characterization of a Ni-rich NiTi alloy bar, produced by Vaccum Induced Melting (VIM) and thermomechanical processing in laboratory scale, aiming at massive production in the future. This study focused on the first step of hot working at 800 ºC during rotary forging. Microstructural characterization was performed using Differential Scanning Calorimetry (DSC), high and low temperature x-ray diffraction (XRD) using a lab source and synchrotron x-ray diffraction (SXRD). Thus, it was possible to obtain the phase transformation characteristics of the material: the transformation temperatures and the transformation sequence. Proposed thermomechanical processing is intended for production of bars and wires that will be subsequently drawn to get thin wires, for different applications, including orthodontic arch wires.

Keywords: Rotary Hot Forging, X-Ray Diffraction, Phase Transformation, NiTi Alloy, Microstructural Characterization

a) Author to whom correspondence should be addressed. Electronic mail: pf.rodrigues@campus.fct.unl.pt

## I. Introduction

Due to their functional properties (shape memory effect and superelasticity) NiTi alloys are very interesting and appealing materials, with applications in medicine, civil engineering and aerospace. (Ramaiah, 2005) (Mohd, 2014)

The singular characteristics of Ni-Ti alloys with composition close to equiatomic are a result of the presence of two phases: austenite (*Strukturbericht* designation: B2; space group $Pm\bar{3}m$), stable at a higher temperature, and martensite (*Strukturbericht* designation: B19'; space group $P2_1/m$), stable at a lower temperature. In some circumstances, an intermediate R-phase (space group $P\bar{3}$) may appear. In the following text, austenite, martensite, and R-phase will be designated by B2, B19', and R, respectively. Transformation temperatures in these alloys may be strongly affected by the Ni/Ti ratio of B2. The superelastic behavior, relevant for the orthodontic application, is a consequence of the stress-induced transformation B2 ⇔ B19'.

The manufacture of these materials is complex, since a variation of the chemical composition and the presence of impurities (e. g. C or O) can drastically change the characteristics of the material. (Frenzel, 2007) (Chu, 1996) (Otubo, 2008) The biggest challenges throughout its processing are the control of the metal matrix composition (ratio Ni/Ti) and the impurity content, such as the carbon and the oxygen, that can give rise to

carbide (TiC) and oxide ($Ti_4Ni_2O$ and $Ti_2O$) inclusions. (Khamei,2010) (Frenzel,2007) (Chu,1996) (Funabuko,1987) (Otsuka, 2005) The presence of carbon or oxygen does not have a direct effect on the transformation temperature; rather, both elements preferentially combine with Ti to form stable compounds, leaving the matrix Ni rich and therefore resulting in a reduction of the transformation temperatures. (Frenzel, 2007) (Chu, 1996) (Frenzel, 2010)

Understanding the behavior of these materials during their manufacturing process is important, especially during the hot deformation steps, such as forging. (Dehghani, 2010) During the hot deformation, cracking may occur as a result of compressive stresses and the presence of inclusions from the previous casting process. (Otubo 2006)

The complexity of the process requires a verification of the functional properties after the applied thermomechanical treatment. The workability of these alloys decreases significantly for temperatures below 800ºC. These difficulties during the hot deformation are related to brittleness and notch-sensitivity. (Morakabati, 2011) So, it is necessary (i) to optimize the hot forging temperature in order to get the best hot-workability and (ii) to guarantee that the metal matrix composition will ensure the stability of B2 in the working temperature range required for orthodontic application, between room temperature and oral temperature (~310K).

A few studies have been devoted to the deformation maps of NiTi alloys K. (Ramaiah, 2005) (Morakabatia, 2011a e 2001b) (Dehghani, 2010a e 2010b) (Morakabatia, 2011) (Khamei, 2010) (Yeom J., 2014)

The aim of the present work is to study the processing route of a Ni-rich NiTi alloy after the first step of rotary hot forging from a processing sequence comprising casting by Vacuum Induction Melting (VIM), remelting and six steps of deformation (4 steps of hot forging and 2 steps of cold-forging). Figure 1 shows the Ni–Ti phase diagram. (Massalski TB, 1990) The composition of the Ni-rich Ni-Ti alloy used in this study (Ni51.03 at% – Ti48.97 at%) is referenced by a dashed-line and the typical range of temperatures used for hot-working is highlighted on the composition line.

In order to use this material for orthodontic wires production, it is required to optimize the hot-workability of the material and to ensure the superelastic behavior close to oral temperature (310 K) at all the stages of the process.

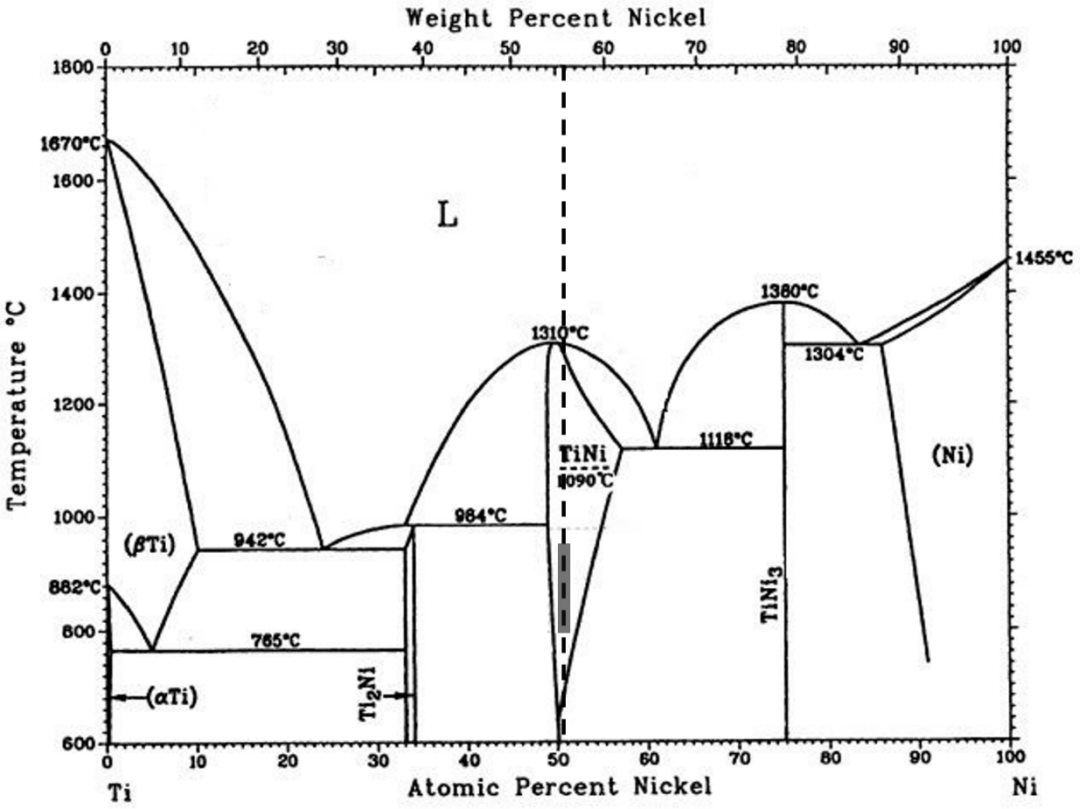


Figure 1. The Ni–Ti phase diagram (adapted from Massalski TB, 1990). The dotted line corresponds to the composition of the alloy used in this study and the grey bar marks the temperature range used for the hot-working of this class of alloys (800 a 950ºC).

## II. EXPERIMENTAL

### A. Material

The sample studied in the present work was obtained from an ingot produced in a VIM furnace under argon atmosphere using a graphite crucible. Subsequently, the ingot was subdivided into smaller pieces, about 90 g each, using electroerosion technique, in order to further recast in the arc melting furnace under argon atmosphere with previous vacuum and argon purge sequence. After being remelted, the ingot was then heated to 800 ºC for 30 minutes. It was then submitted to hot forging, as shown in Figure 2 followed by a slow cooling to room temperature. In the present work it was studied the 1F (First Hot Forging, immediately after the remelting step) sample (Figure 2) (Table I).

The overall chemical composition of the material used in this investigation was determined by WDS: 49.76 at.% of Ni, 47.83 at.% of Ti, 1.88 at.% O and 0.51at.% of C. The following formula [see Eq. (1)] (Otsuka, 1998) has been used for the correction of the effective Ni and Ti content in the metal matrix, taking into account the oxides and carbides formation:

$$\%\boldsymbol{at.Ni(e)} = \frac{(\%\boldsymbol{at.Ni} - \mathbf{0{,}5}\%\boldsymbol{at.O}) \times \mathbf{100}}{((\%\boldsymbol{at.Ni} - (\mathbf{0{,}5} \times \%\boldsymbol{at.O})) + ((\%\boldsymbol{at.Ti} - \%\boldsymbol{at.C} - (\mathbf{0{,}25} \times \%\boldsymbol{at.O}))} \quad (1)$$

Using this formula, the final composition of the metal matrix was estimated to be 48.97 at.% of Ti, 51.03 at.% of Ni.

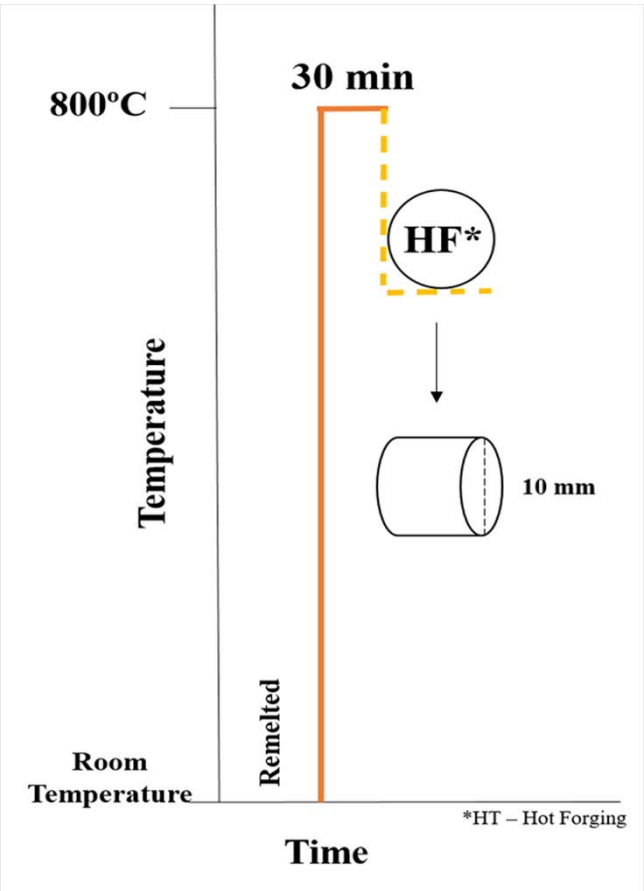


Figure 2. Schematics of the first step of thermomechanical process used in the present study.

Table I. Characteristics of the samples extracted for this study.

| Sample | %at Ni | Diameter | Thickness |
|---|---|---|---|
| Remelting | 51.03 | 18 mm | 5 mm |
| 1F<br>First Hot Forging | 51.03 | 10 mm | 3 mm |

**B. Methods**

The characterization of the transformation temperatures was performed by Differential Scanning Calorimetry (DSC) and the structural characterization by X-Ray Diffraction (XRD).

For the DSC analysis, a DSC 204 F1 Phoenix was used, with thermal cycles from -150 ºC to 150 °C and heating/cooling rate of 10 K/min. Before examination by DSC and XRD, the samples (~ 42 mg) were cut with a low-speed diamond saw and then chemically etched (10vol% HF + 45vol% $HNO_3$ + 45vol% $H_2O$) in order to remove the oxide, as well as the layer deformed by the cutting operation.

For the XRD analysis, a lab source and synchrotron radiation (SXRD) was used.

The lab source was a Bruker X-ray diffractometer (Cu *K*-α radiation). The non-ambient temperature measurements were performed, using a TTK-450 chamber (from Anton Paar), in the range -120 to + 120 ºC at intervals of 10 ºC, during heating and cooling. The $2\theta$ scans covered the range from 36 to 50º ($\delta 2\theta$=0.04º; acquisition 1 sec per point), so that the B2 (110) diffraction peak was observed, as well as other neighboring peaks from

B19'. The texture measurements were performed with an Eulerian Cradle ($0<\chi<69$, $\delta\chi=3$; $0<\phi<360^{o}$, $\delta\phi=3^{o}$) for the (110), (200) and (211) B2 diffraction peaks.
The SXRD experiment was performed in transmission mode using a disc-shaped sample (18 mm diameter for remelting sample and 10 mm diameter for the 1F sample). It was performed at beamline P07 High Energy Materials Science (HEMS) of Petra III/DESY, using a wavelength of 0.1426 Å (87 keV); a beam spot 200 x 200 $\mu m^2$ was used to scan the samples along a diameter (45 points) and a 2D detector Mar345 was placed at 1.35 m from the sample. The raw 2D images were treated using Fit2D program in order to calculate the individual XRD patterns by integration from 0 to 360º.
For the XRD measurement, the identification of the diffraction peaks was based on the ICDD data base. The samples (disc-shaped) used for XRD and SXRD were cut perpendicular to the longitudinal direction of the initial rod.
The XRD and DSC techniques were used in this work to check the structural state of the material and its transformation characteristics. The XRD results give a precise identification of the phases that are present but do not allow a precise definition of the transformation temperatures, due to the temperature steps of 10 ºC between successive holdings. On the other hand, the DSC technique gives a precise definition of the transformation temperature ranges but does not always provide a clear identification of the individual phase transformations due to partial overlapping of transformation peaks. Also, the SXRD gives a local (0.2x0.2 $mm^2$) structural information, but restricted to room temperature. The three techniques provide complementary information about the structural/phase characteristics of the material.

## III. RESULTS AND DISCUSSION

The XRD results show that a two-step phase transformation is taking place during cooling ($B2 \rightarrow R \rightarrow B19'$) and heating ($B19' \rightarrow R \rightarrow B2$) cycles (Figure 3).
For the higher temperature (above to 25ºC), the B2 (110) is clearly visible (Figure 3 -b heating).
During cooling, under 25ºC, there is an abrupt decrease of the B2 (110) peak intensity and two peaks associated to R-phase, close to B2 (110) peak, are noticed. During further cooling, other peaks associated to B19' appear (Figure 3 – a cooling).

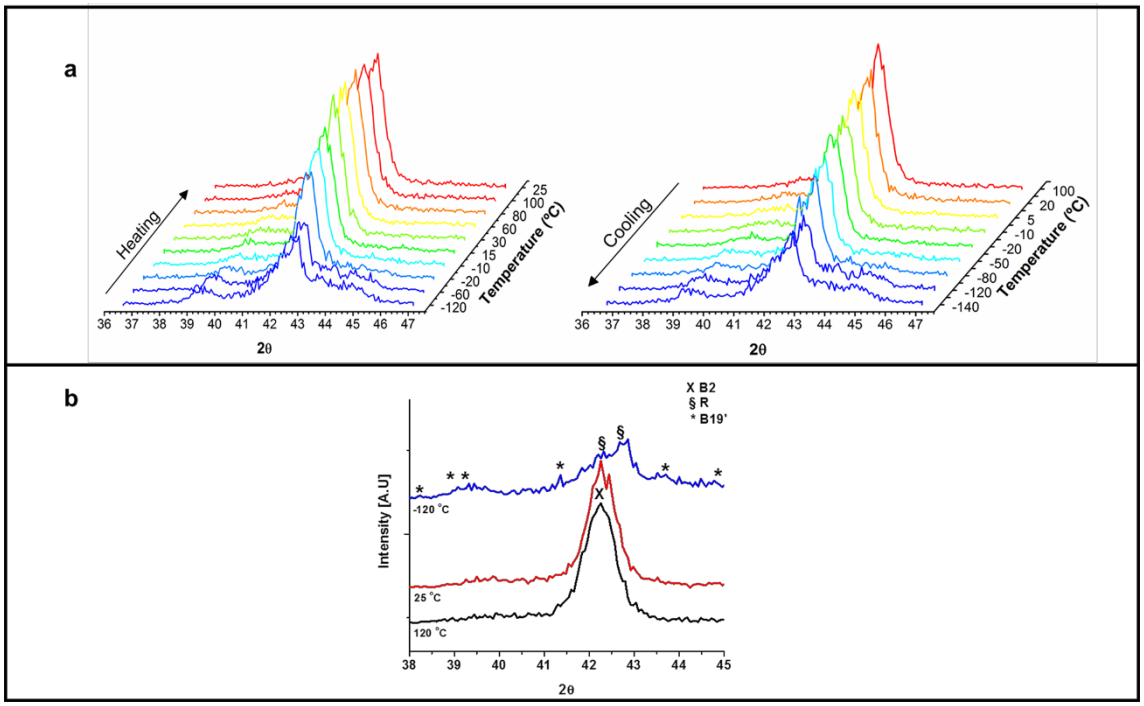


Figure 3. XRD results at high/low temperature: during heating and cooling, between -120 and 120 ºC (a) separate diffractograms for 3 different temperatures (b)

The transformation temperatures were obtained by DSC analysis (Figure 4): the values of transformation temperatures are shown in Table II: austenite start and finish ($A_s$ and $A_f$), during heating, and martensite start and finish ($M_s$ and $M_f$), during cooling. In Figure 4, room temperature is highlighted with a vertical green line, showing that the sample is austenitic slightly above room temperature.

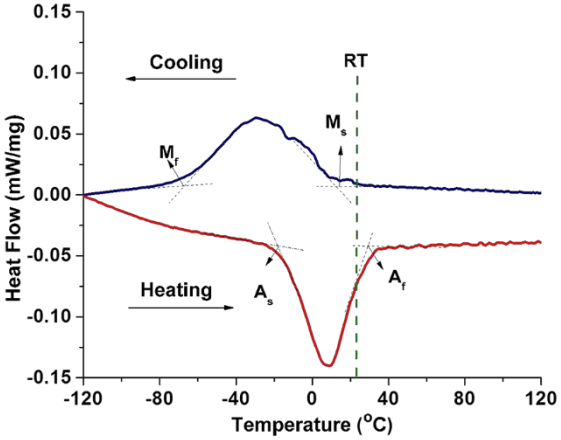


Figure 4. DSC Curve of 1F sample

Table II. Phase transformation temperatures in degree Celsius.

| | Cooling (ºC) | | | Heating (°C) | | |
|---|---|---|---|---|---|---|
| | **$M_s$** | **$M_p$** | **$M_f$** | **$A_s$** | **$A_p$** | **$A_f$** |
| **1F** | 7.2 | -29.4 | -59.0 | -15.1 | 9.2 | 27.5 |

The DSC result shows only one transformation peak on heating and on cooling, suggesting that B2 ⇔ B19' takes place in one single step, but the XRD results clearly show that the intermediate R-phase is formed. Thus, from XRD results, we may conclude that, during cooling/heating, there is a two-step phase transformation (B2 ↔ R ↔ B19').

This piece of information is not evident in DSC results, but it is consistent with the partial overlap of the temperature ranges of DSC peaks during cooling and heating, due to the smaller thermal hysteresis of the B2 ↔ R.
Figure 5 shows the schematic of the measurement along the radial direction using synchrotron radiation. In this scheme, we have isolated three diffraction patterns amongst the 45 points.

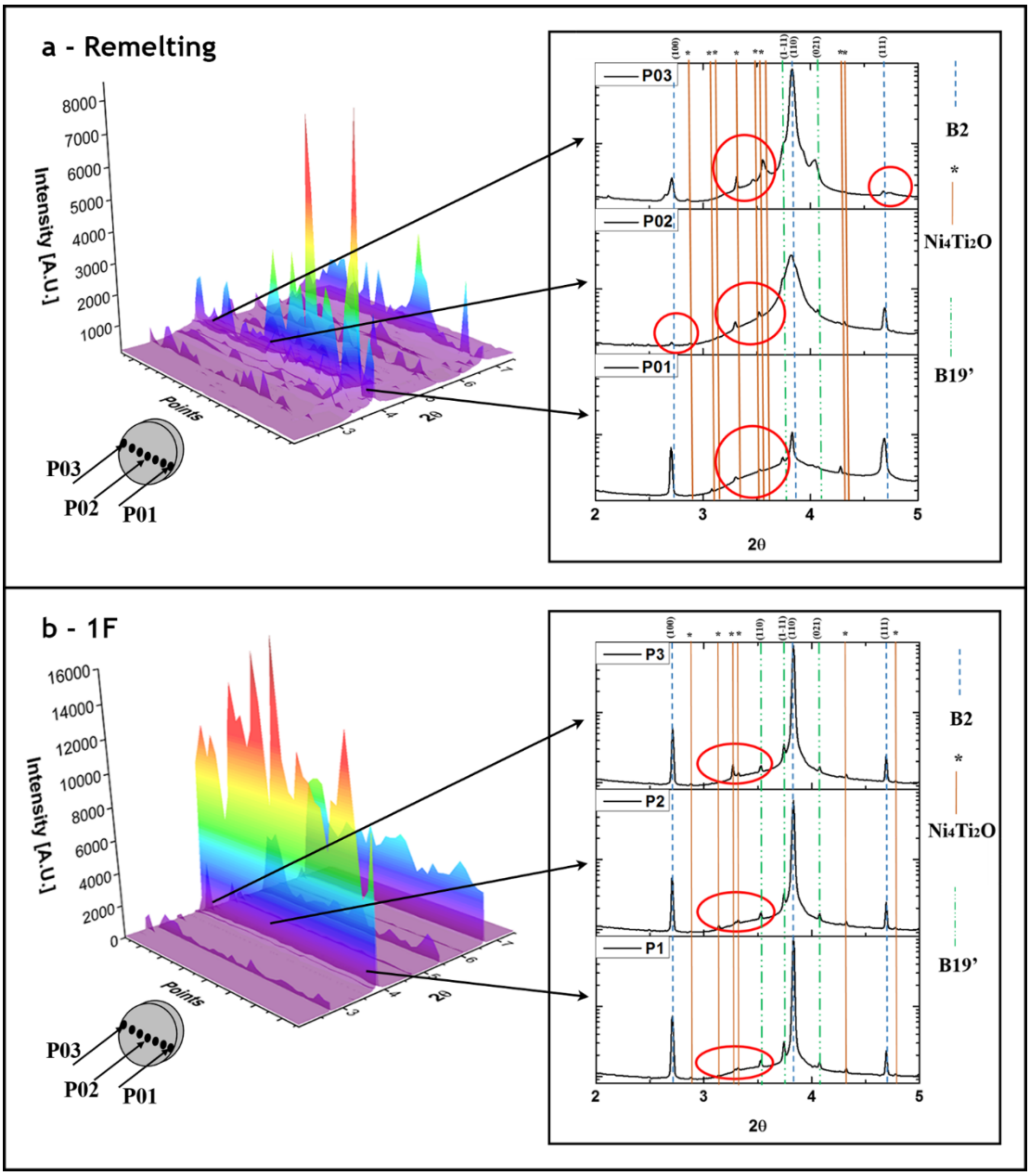


Figure 5. SXRD patterns at room temperature for the sample along the radial direction. a) Remelting b) First step of hot forging (1F). The 3D XRD patterns on the left group the data obtained from 45 points along the diameter for each disc-shaped sample. To the right, 3 diffraction patterns are plotted amongst these 45: P01 and P03, close to the edge of the disc, and P02 at the center.

The SXRD results show an austenitic structure for all points analyzed (Figure 5). This result is consistent with the DSC analysis and the conventional (lab source) XRD result obtained at room temperature. The positions of the $Ni_4Ti_2O$ peaks are highlighted with a

circle (Figure 5). It is possible to observe that, for both samples, we have very different intensities for the B2 peaks. This fact could be associated with the very heterogeneous microstructure after the first hot-forging step (4 hammer forging).
Pole figures (Figure 6) resulting from texture measurements do not indicate a fiber texture, as it is expected to happen at this step of the processing.

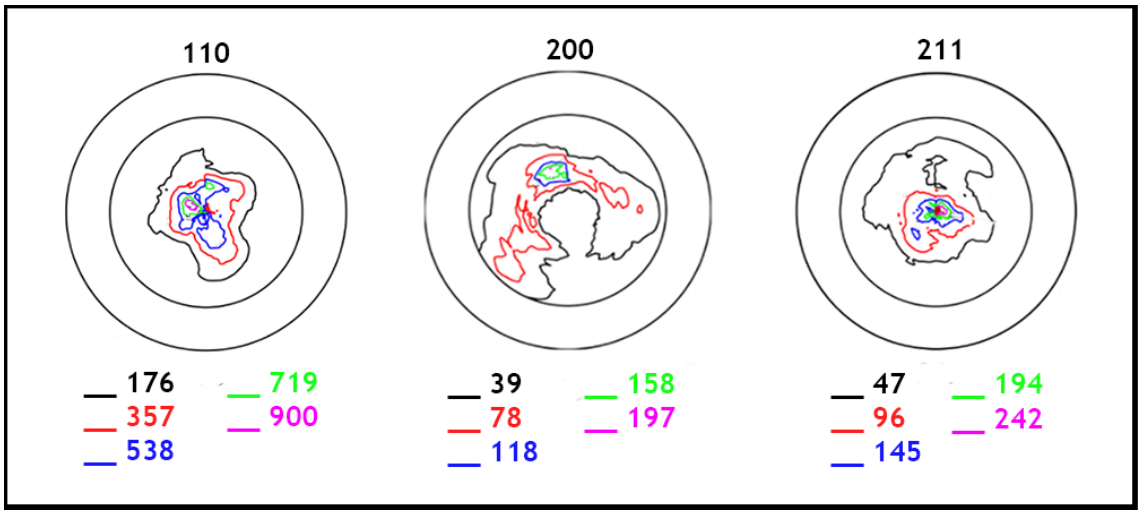

Figure 6. Pole Figures of sample 1F.

## IV. CONLCUSIONS

The analysis of the DSC and XRD results for the first step of the thermomechanical process resulted on:
- the temperature $A_f$ (austenite finish) is close to room temperature; this is relevant for the material to show austenite phase at oral temperature and, thus, show the superelastic behavior required for the application in orthodontic arch wires; this good expectation in terms of functional characteristics was observed after the first step of hot-forging, although a notorious microstructural heterogeneity has been identified by SXRD results;
- the austenite ↔ martensite phase transformation takes place in two steps (B2↔R↔B19');
- the preferential orientation that is present in the rods at the end of the first step of hot forging does not show a fiber texture.
- the XRD results show that, although the material overall behavior is favorable the expected superelastic behavior, the presence of oxides compromises the hot-workability required for further steps of deformation.
These preliminary results show that the chemical composition ensuring the adequate functional properties has been approached, but the casting/remelting steps need to be improved in order to decrease the impurities content (C and O), thus ensuring that a significative improvement of the hot-workability will be reached. Further work is currently following this trend.

## ACKNOWLEDGMENTS
P.F.R, F.M.B.F and J.P.O acknowledge the funding of CENIMAT/I3N by COMPETE 2020, through FCT, under the project UID/CTM/50025/2013.
A.S.P, S.B.R e P.F.R acknowledge the funding of CAPES (APQ-1 2009/02 E-26/110.414/2010, APQ-1 2011-2 E-26/110.269.2012, E-26/111.435/2012 - CsF/ Brazil –

BEX 11943-13-0) and CNPq (research productivity scholarship PQ-2 – Process 307798/2015-1).
The authors thank Professor J. Otubo and postgraduates J.P.Toseti and G.H.T.A. da Silva, for donating the starting materials, and support in the use of the infrastructure of the Institute of Aeronautical Technology to achieve the melting and forging process conditions adopted in this work.

**REFERENCES**

- Chu C.L., Wu S.K., Yen Y.C. **(1996)**, "Oxidation behavior of equiatomic TiNi alloy in high temperature air environment." Materials Science and Engineering A **216**,193-200
- Dehghani K., Khamei A.A., **(2010a)** "Hot deformation behavior of 60Nitinol ($Ni_{60\ wt\%}$–$Ti_{40\ wt\%}$) alloy: Experimental and computational studies." Materials Science and Engineering A **527**, 684–690.
- Dehghani K., Khamei A.A. **(2010b)**, "Modeling the hot-deformation behavior of Ni60 wt%–Ti40 wt% intermetallic alloy.", Journal of Alloys and Compounds **490**, 377–381
- Frenzel J, Zhang Z, Somsen C, Neuking K, Eggeler G. **(2007) "**Influence of Carbon on Martensitic Phase Transformations in Niti Shape Memory Alloys." Acta Materialia **55** 1331–1341
- Frenzel J., George E.P., Dlouhy A., Somsen Ch., Wagner M.F.-X., Eggeler G., **(2010)**, "Influence of Ni on martensitic phase transformations in NiTi shape memory alloys, Acta Materialia **58**, 3444–3458
- Funakubo H. **(1987)** In: Shape Memory Alloys, Vol. 1. Science Publishers (New York: Gordon And Breach).
- Jong-Taek Yeom, Jeoung Han Kim, Jae-Keun Hong, Seong Woong Kim, Chan-Hee Park, Tae Hyun Nam, Kee-Young Lee. **(2014)** "Hot forging design of as-cast NiTi shape memory alloy." Materials Research Bulletin **58**, 234-238
- Khamei A., Dehghani K., **(2010a)** Microstructural evolution during the hot deformation of Ti-55Ni (at. pct) intermetallic alloy, Metallurgical and Materials Trans- actions A **41** 2595–2605.
- Khamei A.A., Dehghani K. **(2010b)**, "A study on the mechanical behavior and microstructural evolution of Ni60 wt%–Ti40 wt% (60Nitinol) intermetallic compound during hot deformation", Materials Chemistry and Physics **123**, 269–277
- Massalski TB, Okamoto H, Subramanian PR, Kacprzak L, **(1990)** editors. Binary alloy phase diagrams, 2nd edition, vol. **3**. Materials Park, OH: ASM International 2874.
- Mohd Jani J., Leary M., Subic A., Gibson M.A. **(2014)**, "Review: A review of shape memory alloy research, applications and opportunities, Materials and Design, **56**, 1078-1113
- Morakabatia M., Kheirandisha, Sh., Aboutalebia M., Karimi Taherib A., Abbasic S.M. **(2011a)**, "A study on the hot workability of wrought NiTi shape memory alloy." Materials Science and Engineering A **528,** 5656–5663
- Morakabati M., Aboutalebi M., Kheirandish Sh., Karimi Taheri A., Abbasi S.M. **(2011b)**, "High temperature deformation and processing map of a NiTi intermetallic alloy.", Intermetallics **19**, 1399e1404
- Otsuka, K.; Wayman, C.M. **(1998)**, "Shape Memory Materials", Cambridge University Press.
- Otsuka K., Ren X., **(2005) "**Physical metallurgy of Ti–Ni-based shape memory

alloys", Prog. Mater. Sci., **516**, 669.
- Otubo J., Rigo O.D., Moura Neto C., Mei P.R. **(2006)**,"The effects of vacuum induction melting and electron beam melting techniques on the purity of NiTi shape memory alloys.", Materials Science and Engineering A **438–440** 679–682
- Otubo J., Rigo O.D., Coelho A.A., Neto C.M., Mei P.R., **(2008)** "The influence of carbon and oxygen content on the martensitic transformation temperatures and enthalpies of NiTi shape memory alloy.", Materials Science and Engineering A **481–482**, 639–642
- Ramaiah KV, Saikrishna CN, Bhaumik SK, **(2005)** "Processing of Ni-Ti Shape Memory Alloy Wires." International Conference of Smart Materials Structures and Systems 2005:SC141
- Suresh K.S., Bhaumik Subir K., Satyam Suwas **(2013)**, "Effect of thermal and thermo-mechanical cycling on the microstructure of Ni-rich NiTi shape memory alloys.", MaterialsLetters **99,** 150–153

Table I. Characteristics of the samples extracted for this study.

| Sample | %at Ni | Diameter | Thickness |
|---|---|---|---|
| Remelting | 51.03 | 18 mm | 5 mm |
| 1F<br>First Hot Forging | 51.03 | 10 mm | 3 mm |

Table II. Phase transformation temperatures in degree Celsius.

| | Cooling (°C) | | | Heating (°C) | | |
|---|---|---|---|---|---|---|
| | **$M_s$** | **$M_p$** | **$M_f$** | **$A_s$** | **$A_p$** | **$A_f$** |
| **1F** | 7.2 | -29.4 | -59.0 | -15.1 | 9.2 | 27.5 |

Figure 1. The Ni–Ti phase diagram (adapted from Massalski TB, 1990). The dotted line corresponds to the composition of the alloy used in this study and the grey bar marks the temperature range used for the hot-working of this class of alloys.

Figure 2. Schematics of the first step of thermomechanical process used in the present study.

Figure 3. XRD results at high/low temperature: during heating and cooling, between -120 and 120 ºC (a) separate diffractograms for 3 different temperatures (b)

Figure 4. DSC Curve of 1F sample.

Figure 5. SXRD patterns at room temperature for the sample along the radial direction. a) Remelting b) First step of hot forging (1F). The 3D XRD patterns on the left group the data obtained from 45 points along the diameter for each disc-shaped sample. To the right 3 diffraction patterns are plotted amongst these 45: P01 and P03, close to the edge of the disc, and P02 at the center.

Figure 6. Pole Figure of sample 1F.